

## 3-D magnetic configurations supporting prominences

### I. The natural presence of lateral feet

G. Aulanier and P. Démoulin

Observatoire de Paris, section Meudon, DASOP, URA 2080 (CNRS), F-92195 Meudon Principal Cedex, France

Received 23 May 1997 / Accepted 27 August 1997

**Abstract.** It is now commonly accepted that prominence plasma is supported in magnetic dips, in particular in twisted flux-tubes. But present two-dimensional models are unable to explain the observed presence and structure of prominences feet. This requires three-dimensional models.

We modeled the field using linear force-free field equations. Combining a small number of harmonics, and using observational constraints, we have found the area in the parameter space where prominences are likely to be present. Then, adding 3-D harmonics, we show that feet appear periodically underneath the prominence body. For great helicity, the parameter space is mostly fulfilled by configurations which have feet alternating between both sides of the prominence axis, as observed. The theoretical photospheric field has a quasi-bipolar pattern and the prominence stands above a magnetic corridor containing only small parasitic polarities. The lateral feet are formed by dips in the vicinity of these small polarities. These configurations show in a natural fashion a number of well-established as well as more recent observational aspects of prominences, in particular the vector magnetic field measurements in prominences and the chirality patterns (the dextral/sinistral, right/left bearing, skew of the overlying coronal arcade and fibril organization in prominence channels).

**Key words:** MHD – Sun: prominences – filaments – magnetic fields

---

#### 1. Introduction

Prominences are thin structures consisting of cold plasma embedded in the hot corona. Their global shape has been known since a long time (e.g. d’Azambuja & d’Azambuja 1948). Prominences consist of bridges of chromospheric-like material located in the corona. Periodically the prominence connects to the photosphere by, so called feet or barbs, similar to road bridges. In this paper we use the term “feet”, rather than “barbs”,

because in the model that we describe the dense material is supported while the term “barbs” was used by Martin et al. (1994) in the context of absence of dips, i.e. magnetic support. (More specific observations of the prominence morphology are introduced below in comparison with the model.)

Prominences are always found above inversion lines of the photospheric magnetic field in regions, called corridors or filament channels, which are nearly free of chromospheric fibrils (Martres et al. 1966). They are also characterized on either side by the presence of  $H\alpha$  fibrils nearly aligned with the inversion line, indicating a high magnetic shear (Foukal 1971; Rompolt 1990). The corridor is nearly free of vertical magnetic field flux except of small parasitic polarities (Martin 1990). A necessary condition for prominence formation is a low gradient transverse to the photospheric inversion line, of the vertical field component (Shelke & Pande 1983; Maksimov & Ermakova 1985; Maksimov & Prokopiev 1995).

In prominences the Zeeman effect only allows the measurement of the longitudinal component of the magnetic field (see Kim 1990 and references therein). The Hanle effect gives the three components of the field (and the electron density) from the polarization measurements in two spectral lines (e.g. Bommier et al. 1994). The compatibility of the results obtained by these two independent methods and by different groups of observers has strongly contributed to validate their respective results (see the reviews of Leroy 1988, 1989 and Kim 1990). It is now well accepted (since Athay et al. 1983), while compatible with a slight dip configuration (Bommier et al. 1986, 1994). The magnetic field strength is nearly homogeneous (Leroy 1989) at the scale of few arc seconds, but show a statistical increase of strength with height which is compatible with a dip configuration (e.g. Leroy et al. 1983). One main result of Hanle measurements is that the prominence field has the opposite direction to the one expected from extrapolation of photospheric measurements (e.g. Leroy et al. 1983). Not only the field component orthogonal to the prominence is opposite to the field of a simple arcade (referred as an Inverse configuration), but also the field component parallel to the prominence is opposite to those of an arcade that would have been sheared by differential rotation ! A large majority of

---

*Send offprint requests to:* G. Aulanier

prominences are in the Inverse type (75% in Leroy et al. 1984, 85% in Bommier et al. 1994 and greater than 90% in Bommier & Leroy 1997).

Because the plasma  $\beta$  is low in the corona as in prominences, the magnetic field plays a key role in all the processes involved. It channels both the plasma motions and the thermal conduction. It allows support against gravity of the prominence plasma one hundred times denser than the coronal plasma. In the present paper we will emphasize the importance of this last point and show that the necessity of magnetic support (in magnetic dips) naturally implies the observed 3-D shape of prominences, in particular the presence of lateral feet.

The gravitational scale height of prominence material is much lower than the typical height of prominences. This implies that gas pressure cannot be the mechanism of support. The observed velocities (few  $\text{km s}^{-1}$ ) are much less important than the free-fall velocities (several  $10 \text{ km s}^{-1}$ ) and usually, the velocity maps do not show a pattern similar to the one seen in arch filament systems (Schmieder 1989). Then the cold prominence plasma should be supported by the magnetic field. If enough mass (i.e. a plasma beta greater than 0.05) can be brought at the top of sheared magnetic arcade in less than one hour, the gravity force can bend down at the top of the arcade, providing a stable support to the prominence plasma (Schmieder et al. 1991; Fiedler & Hood 1993). However prominence formation takes usually a few days (resp. few weeks) for prominences in (resp. outside) active regions (e.g. Malherbe 1989). It implies that a magnetic dip should be present in the magnetic configuration before any dense material can slowly accumulate there.

The need of a magnetic dip for stable support was first pointed out by Kippenhahn & Schlüter (1957), however, the implications of such a condition were used only recently to select magnetic configurations suitable for prominence formation (see Priest et al. 1989 for developments). Apart from quadrupolar regions, where a dip is naturally present between the two bipoles, usually a dip is not present in a simply connected bipolar region. For instance, Amari et al. (1991) have proved that, in a bipolar region, a 2.5-D force-free field with an arcade topology cannot have a dip. This is however possible in 3-D with a overlying arcade compressing locally the central-part of an underlying sheared arcade (Antiochos et al. 1994). Another way to create a dip is to form a twisted configuration (e.g. in a 2.5-D linear force-free field, Démoulin & Priest 1989). Twisted configurations can be formed in several ways: by photospheric twisting motions (Priest et al. 1989), by converging motions in a sheared arcade with magnetic reconnection at the inversion line (van Ballegooijen & Martens 1989; Choe & Lee 1992), by resistive instability in an sheared arcade (e.g. Inhester et al. 1992), by relaxation and accumulation of helicity (e.g. Rust & Kumar 1994) or by emergence with inherent twist from the convective zone (e.g. Low 1994).

Twisted configurations are promising magnetic configurations for prominences, in particular because dense material can be naturally supported in them and because there are observational evidences of them (mainly in prominence eruptions, e.g. Raadu et al. 1988; Vršnak et al. 1991). Our aim in this paper

is to go further than this usual statement by showing that 3-D twisted configurations permit to interpret a variety of observations within a single magnetic configuration. After a summary of the method in Sect. 2, we first analyze configurations invariant by translation in Sect. 3 with the aim to classify the variety of possible topologies in the parameters space. We then analyze examples of 3-D magnetic configurations in the Sect. 4 and show that the simple dip constraint leads naturally to the formation of prominence feet. Finally, in Sect. 5, we confront the properties of our model magnetic configurations with a variety of observed features of prominences.

## 2. Description of the model

### 2.1. Assumptions

Prominences are formed of plasma sufficiently ionised and dense that we can consider the plasma (and the neutral elements) frozen in the magnetic field. Furthermore, their long-time existence and the slow motions of the plasma inside them, allows us to consider their global structure as quasi-static, in a first approximation. The plasma  $\beta$  is typically of the order of 0.01–0.1, so the field can almost be considered as force-free. We choose below a linear force-free field because we want to have a large class of 3-D equilibrium to understand the presence of feet. As emphasized in Sect. 1, the main criterion for a magnetic configuration that can support a prominence is the existence of dips in the field lines. In the following we will suppose that cold material is present in such dips while we neglect its effect on the magnetic field.

### 2.2. Three-dimensional linear force-free field solutions

A linear force free field satisfies:

$$\nabla \times \mathbf{B} = \alpha \mathbf{B}, \quad (1)$$

$$\nabla \cdot \mathbf{B} = 0, \quad (2)$$

with  $\alpha = \text{constant}$ . This leads to the differential equation:

$$\Delta \mathbf{B} + \alpha^2 \mathbf{B} = 0. \quad (3)$$

We use a cartesian system of coordinates, where  $z$  refers to the height,  $y$  to the prominence axis, and  $x$  to the direction perpendicular to the prominence. The solution of Eq. (3) can be expressed in periodic harmonics for the field in the  $x$  and  $y$  directions, as shown in previous works (Nakagawa & Raadu 1972 and Démoulin et al. 1989).  $L_x$  and  $L_y$  are the periodicity of the field in the  $x$  and the  $y$  directions. We assume a dependence of the field in the vertical direction as  $e^{-lz}$ , so that the magnetic field decreases with height. We avoid the solutions that give a dependence like  $e^{lz}$ , because they give non-physical results. For the vertical component of the field, we only keep the solution that behaves like  $\sin(k_x x)$ , so this gives an odd solution in the  $x$  direction. Hence, the inversion line for the photospheric field stands at  $x = 0$ , which is easy to deal with. The harmonics for

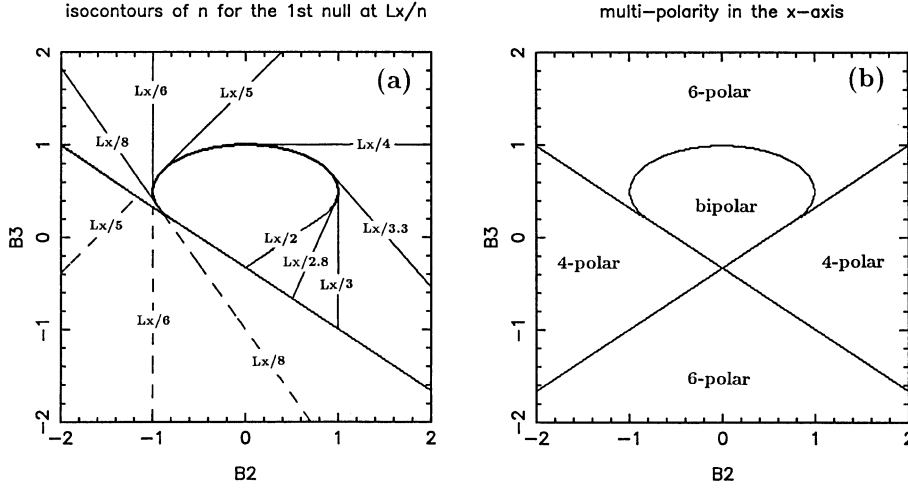


**Fig. 1a and b.** The isocontours of the first null value for the photospheric  $B_z$  between  $x = 0$  and  $x = Lx/2$  are reported on **a** for various values of the amplitude  $\tilde{B}_2$  and  $\tilde{B}_3$  with  $\tilde{B}_1 = 1$ . Full lines (dashed lines) mean that  $B_z(z = 0) > 0$  ( $< 0$ ) between  $x = 0$  and the first null. The number of photospheric magnetic field polarities between  $x = -Lx/2$  and  $x = Lx/2$  is reported on **b**.

the magnetic field are then given by:

$$B_x = \frac{\tilde{B}_{(n_x; n_y)}}{k_x^2 + k_y^2} \left( -\alpha k_y \sin(k_x x) \sin(k_y y) - l k_x \cos(k_x x) \cos(k_y y) \right) e^{-lz}, \quad (4)$$

$$B_y = \frac{\tilde{B}_{(n_x; n_y)}}{k_x^2 + k_y^2} \left( l k_y \sin(k_x x) \sin(k_y y) - \alpha k_x \cos(k_x x) \cos(k_y y) \right) e^{-lz}, \quad (5)$$

$$B_z = \tilde{B}_{(n_x; n_y)} \sin(k_x x) \cos(k_y y) e^{-lz}. \quad (6)$$

with  $\tilde{B}_{(n_x; n_y)}$  is the amplitude of the harmonic  $(n_x; n_y)$ , and

$$k_x = n_x \cdot 2\pi / L_x, \quad (7)$$

$$k_y = n_y \cdot 2\pi / L_y \quad (8)$$

$$l = \sqrt{k_x^2 + k_y^2 - \alpha^2}. \quad (9)$$

From Eq. (9) we see that  $\alpha$  has a maximum value  $\alpha_{max} = 2\pi / L_x$  ( $n_x \geq 1, n_y \geq 0$ ). For  $\alpha > \alpha_{max}$ ,  $e^{-lz}$  becomes an oscillating solution with height, which is not physical. So we restrict ourselves to  $\alpha < \alpha_{max}$ . In the following, the values given for  $\alpha$  are normalized to  $\alpha_{max}$ . So the value of  $\alpha$  in Mm will be:

$$\alpha(\text{Mm}) = \alpha(\text{normalized}) \frac{2\pi}{L_x}. \quad (10)$$

### 2.3. The criterion for dips in the field lines

In this section we derive the expression of the curvature of a field line as a function of the magnetic-field spatial derivatives. Rather than using the properties of a force-free field, we use the general definition for the curvature of a field line. Let  $(\mathbf{u}_t, \mathbf{u}_n, \mathbf{u}_b)$  be the local Frenet vector base associated to a field line path ( $\mathbf{u}_t$  is the local tangent, and  $\mathbf{u}_n$  the local curvature direction). We note  $R_c$  the curvature radius of the field line, and  $s$  the arc length on field lines. Then we can write:

$$\frac{\mathbf{u}_n}{R_c} = \frac{d\mathbf{u}_t}{ds} = \frac{d(\mathbf{B}/B)}{ds}. \quad (11)$$

The field line equation is given by:

$$\frac{dx}{B_x} = \frac{dy}{B_y} = \frac{dz}{B_z} = \frac{ds}{B}. \quad (12)$$

Whatever is the variable  $a(x, y, z)$ , we can write that

$$\frac{da}{ds} = \frac{dx}{ds} \frac{\partial a}{\partial x} + \frac{dy}{ds} \frac{\partial a}{\partial y} + \frac{dz}{ds} \frac{\partial a}{\partial z}. \quad (13)$$

Then, combining Eq. (12) and (13), we easily get to:

$$\frac{da}{ds} = \frac{\mathbf{B}}{B} \cdot \nabla a \quad (14)$$

Introducing the result of Eq. (14) in Eq. (11) we reach:

$$\frac{\mathbf{u}_n}{R_c} = \frac{(\mathbf{B} \cdot \nabla) \mathbf{B}}{B^2} - \frac{\mathbf{B}}{B^3} (\mathbf{B} \cdot \nabla) B. \quad (15)$$

In general, it is not easy to deal with this equation, but in our case, we are only interested in the curvature of the field lines where  $B_z(x, y, z) = 0$ . In this condition, we finally obtain:

$$\frac{\mathbf{u}_n}{R_c} \cdot \mathbf{u}_z = \frac{1}{B^2} \left( B_x \frac{\partial B_z}{\partial x} + B_y \frac{\partial B_z}{\partial y} \right). \quad (16)$$

### 3. Results for a two-dimensional configuration

We use a small number of harmonics to describe the magnetic field in the prominence to catch the main topological features. This also allows us to make a systematic study how the configuration evolves as we modify the various parameters involved. Démoulin & Priest (1989) have shown that it is possible to form a twisted configuration even with only two harmonics of the 2.5-D linear force-free field. For  $|\alpha|$  great enough, the  $B_x$  component of the second harmonic can dominate the component of the first one at low height, creating an inverse configuration with a dip. With a third harmonic, Amari & Aly (1992) show that it is possible to form a twisted region detached from the lower boundary (photosphere). Passing alternatively between these two basic configurations permits intuitively to have an alternation of feet. However, before the analysis of fully 3-D configurations a preliminary 2.5-D study is necessary, in order to find every configuration satisfying the conditions for prominence support.

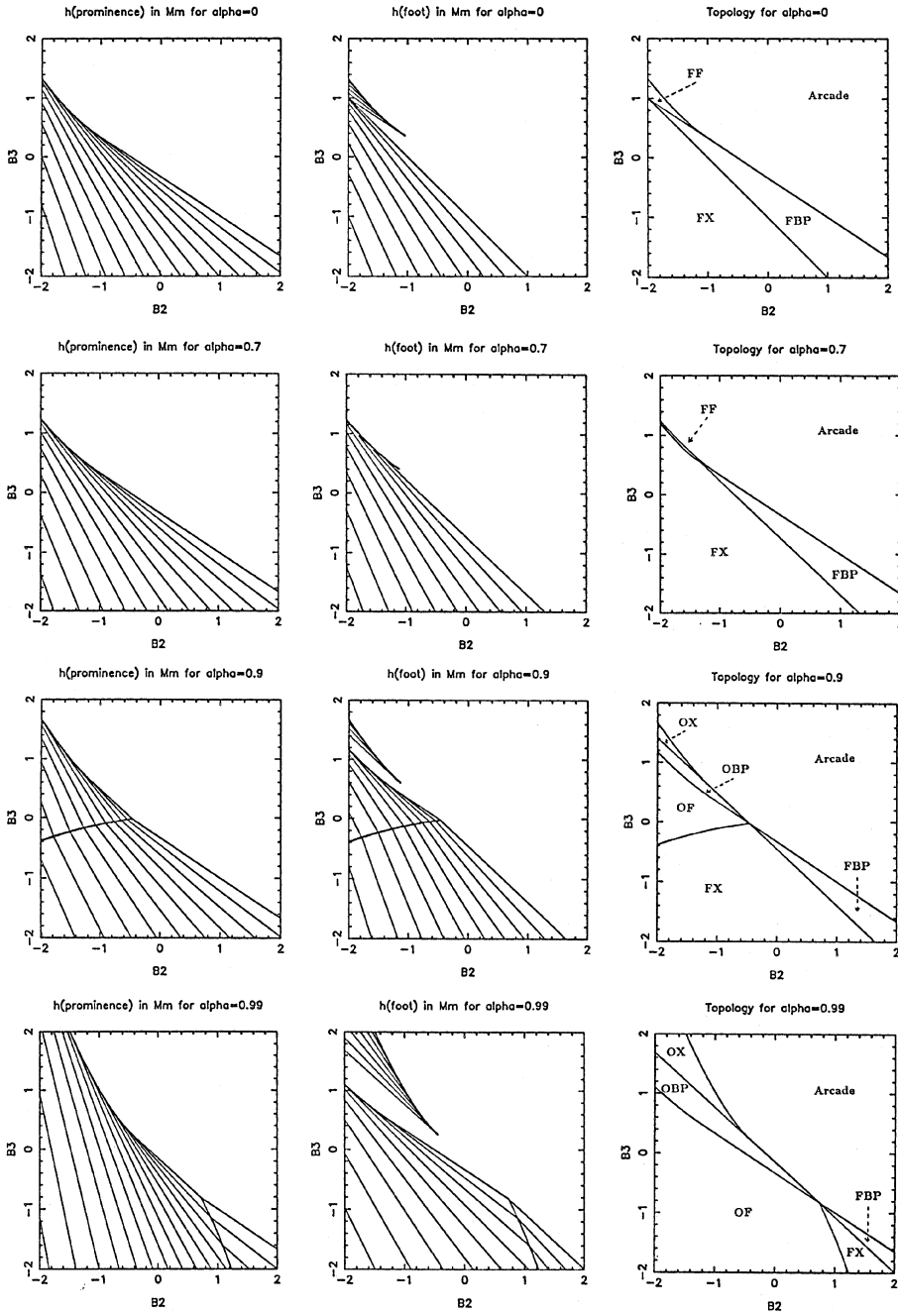


**Fig. 2.** Isocontours for the height of the top (1st column) and bottom (2nd column) of the prominence, and topology (3rd column) of the 2.5-D field, for various values of  $\alpha$ . Note the reverse line between OF and FX that moves with increasing values of  $\alpha$  (see text). The isocontours of height start from 0, and are drawn with  $L_x/50$  intervals (hence for  $L_x = 100$  Mm, isocontours are drawn every 2 Mm). On each diagram, the isocontours value increases as  $\tilde{B}_2$  and  $\tilde{B}_3$  decrease, except where there topology is FF or OX. There, the isocontours value increases as  $\tilde{B}_2$  and  $\tilde{B}_3$  increase.

### 3.1. Combination of harmonics

In 2.5-D, the magnetic configuration is invariant along the  $y$  axis. Hence, the harmonics for the magnetic field given by Eq. (4), 5 and 6 can be expressed as:

$$B_x(n_x) = -\frac{l\tilde{B}_{(n_x)}}{k_x} \cos(k_x x) e^{-lz},$$

$$B_y(n_x) = -\frac{\alpha\tilde{B}_{(n_x)}}{k_x} \cos(k_x x) e^{-lz},$$

$$B_z(n_x) = \tilde{B}_{(n_x)} \sin(k_x x) e^{-lz}.$$

We combine three harmonics, given by  $n_x = 1, 2, 3$  assuming that the amplitude of the first one is  $\tilde{B}_1 = 1$ . Then the three components of the magnetic field are given by:

$$B_{x,y,z} = \sum_{n_x=1}^3 B_{x,y,z}(n_x). \quad (20)$$

(17) There are many parameters in such an approach. We decide to vary the amplitudes  $\tilde{B}_{(n_x)}$  of the harmonics.

### (18) 3.2. The polarity of the photospheric field

(19) As we want to understand observations, we are looking for a photospheric vertical field which is mainly bipolar, with a low

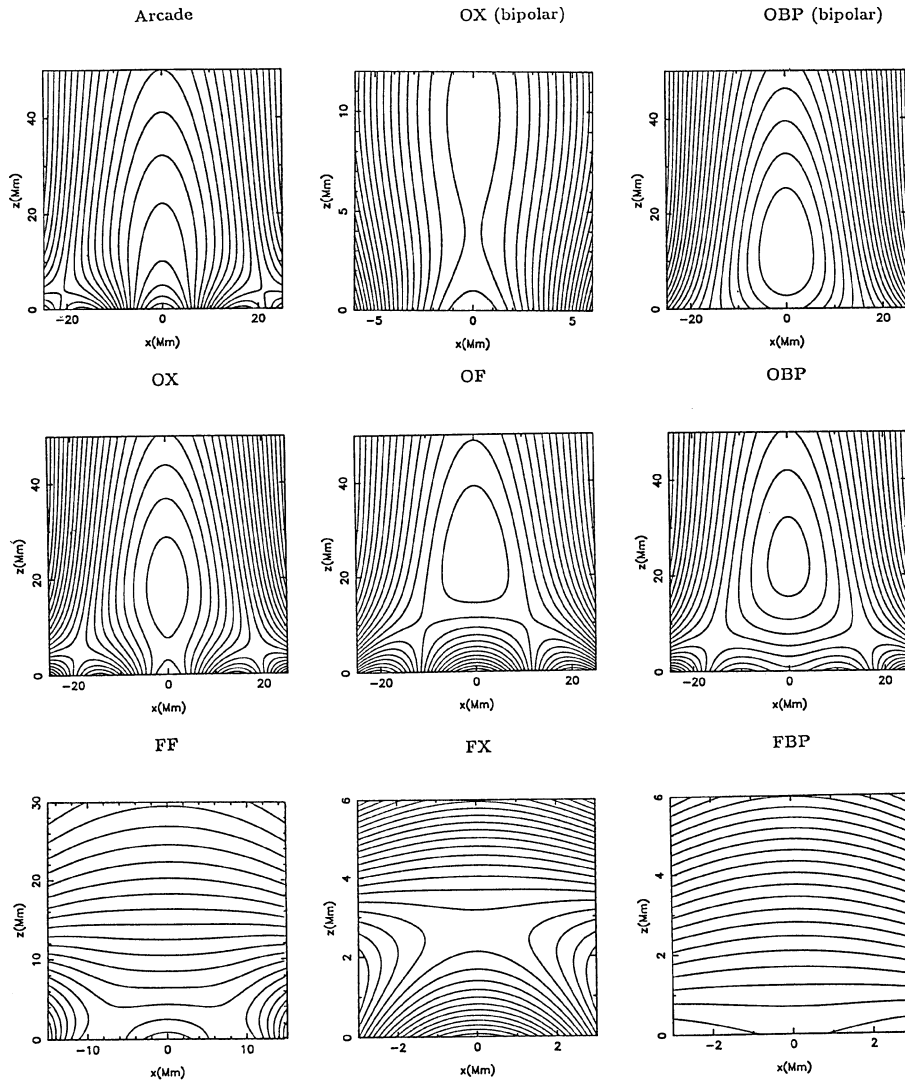


**Fig. 3.** Different topologies for the field in 2.5-D. The first letter of the terminology refers to the top of the prominence (dip location), and the second one to its bottom. F is given for flat field line, O for O-point (so a twisted flux tube), X for X-point and BP for bald patches. The field lines are drawn with  $L_x = 100$  Mm.

field region around the inversion line. In order to do so, we investigate the locations where  $B_z = 0$  at the level  $z = 0$  (photospheric level). In Fig. 1a and b the global behavior of the vertical component of the magnetic field at the photospheric level is reported. The choice we made for the used harmonics naturally leads to the three kinds of configurations shown in Fig. 1a and b. Within one period of the field along the  $x$  axis, between  $-L_x/2$  and  $L_x/2$ , we find two sextupolar regions, two quadrupolar, and one bipolar for low values of  $\tilde{B}_2$  and  $\tilde{B}_3$ . They are bounded by two lines and one ellipse, which equations are:

$$3\tilde{B}_3 + 2\tilde{B}_2 = -1, \quad (21)$$

$$3\tilde{B}_3 - 2\tilde{B}_2 = -1, \quad (22)$$

$$\tilde{B}_2^2 + 4\left(\tilde{B}_3 - \frac{1}{2}\right)^2 = 1. \quad (23)$$

This diagram is similar to the one found by Amari & Aly (1992); it differs only because we are using the magnetic field (rather than its potential) and the three first harmonics (rather than the first, third and fifth ones). This result gives us some first constraints on the amplitude of the harmonics we need for a suitable

prominence, because we have to remain close to a bipolar configuration.

### 3.3. Basic topology for a 2.5-D configuration

Here we investigate the various typical vertical sizes for a 2.5-D prominence, such as the height of its top and bottom. In order to do so, we calculate the values of  $z$  where the field lines present a dip above the inversion line, at  $x = 0$ . For a configuration which is invariant along the  $y$  axis, the condition for having a dip in a field line at a given height  $z_{dip}$  is (from Eq. (16)):

$$\left. \frac{B_x}{B^2} \frac{\partial B_z}{\partial x} \right|_{z=z_{dip}} > 0. \quad (24)$$

The two first columns in Fig. 2 show respectively isocontours for the height of the top, and for the bottom, of the prominence, as  $\tilde{B}_2$ ,  $\tilde{B}_3$  and  $\alpha$  vary. We assume that the prominence exists between these two values. One can see that whatever is  $\alpha$ , no prominence exists for large values of  $\tilde{B}_2$  and  $\tilde{B}_3$ . There are also some configurations for which the height of the bottom is

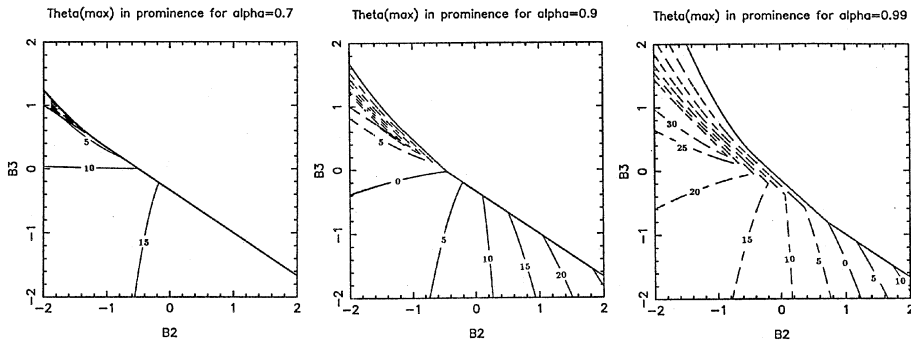


**Fig. 4.** Maximum value of the angle between the field inside the prominence at  $x = 0$ , at the inversion line, for various values of  $\alpha$ , with  $\tilde{B}_{1,1} = 0$ ,  $\tilde{B}_{2,1} = 0.3$  and  $\tilde{B}_{3,1} = -0.7$ . Full lines are given for normal polarity configurations, and dashed lines for inverse polarity; they are separated by the reverse line as seen in Fig. 2. Note that even for high values of  $\alpha$ , it is possible to keep a large angle in the prominence.

zero. It can be guessed that the feet of the prominence will have such a configuration. From these figures, we can see that the prominence is higher for lower  $\tilde{B}_2$  and  $\tilde{B}_3$ . This is also true for its bottom, except for high values of  $\tilde{B}_3$ , where the bottom of the prominence rises again with  $\tilde{B}_3$ , after having crossed a region where its height is zero.

The topology of the field lines above the inversion line is shown in the third column in Fig. 2. There are nine possible topologies for the conditions we use in this paper. The explanation of the terminology that describes the different regions in Fig. 2 is given in Fig. 3. The prominence bottom is formed whether by a dip whose field line is tangent to the photosphere (defined as a bald patch by Titov et al. 1993), or an X-point, or a flat field line. Its top part is composed of an O-point or another flat field line. Such results are comparable with those of Amari & Aly (1992). The corresponding notations are  $C_0K_0$  for Arcade,  $C_0K_1$  for FBP,  $C_0K_2$  for FF,  $C_1K_0$  for OBP,  $C_1K_1^+$  for OF,  $C_1K_1^-$  for FX and  $C_2K_0$  for OX. The combination of three harmonics highlights that if the bottom of the prominence is due to a flat field line belonging to a twisted flux tube, there are two X-points at some distance on both sides of the inversion line. This is due to the appearance of small parasitic polarities around the inversion line.

### 3.4. Modification of the topology with $\alpha$

The FX topology is dominant for low values of  $|\alpha|$ . But for  $|\alpha| > 0.85$  (normalized value), the OF topology region appears (in the region shown in Fig. 2), and gradually extends in the FX region with increasing  $|\alpha|$ . In this shrinking FX region, the isocontours for the bottom and for the top of the prominence are almost parallel and have nearly equal value. Hence, FX prominences for high  $|\alpha|$  have a short vertical extent. They are either at very low altitude, or very thin. Matter supported in such a thin layer is unlikely to be observed as a dark filament in absorption on the disk. It follows that FX prominences, with a normal polarity configuration, necessarily have quite a small  $|\alpha|$ , as far as modeling in the linear force-free field approximation shows.

Furthermore, at approximately for the same critical value of  $|\alpha|$ , the little FF region disappears completely, leaving its place for a growing OX region. This is an important point, because it shows that O-points only appear for very high values

of  $|\alpha|$ . They are the signatures of twisted flux tubes, leading to inverse polarity configuration for prominences.

For high values of  $|\alpha|$ , one can notice a transition region, going from FX to OF. This curve evolves with  $\alpha$ , gradually crossing the graph and it induces a discontinuity in the isocontour curves (see Fig. 2, first and second column). We call this curve the reverse line. Crossing this line from the FX to the OF configuration implies several changes. First, the height of the top of the prominence becomes equal to those of its bottom, which means that the vertical thickness of the prominence becomes zero. Then, the 2-D topology around  $x = 0$  evolves from one X-point to two X-point plus an O-point. The field becomes twisted. Finally, the configuration passes from normal polarity to inverse polarity.

### 3.5. The lateral dip structure

It has already been emphasized that the underlying feet structure of the prominence could be modelled by bald patches, but looking aside from the inversion line, one can notice that there are some secondary dips for the OF and the FF topologies (see Fig. 3). This is due to the presence of X-points (in the  $x$ - $z$  plane) on both sides of the main prominence body. They are indeed created by some small parasitic polarities in a low field region around the inversion line. Then we can assume that some cold matter can also be supported here against gravity, leading to a lateral feet structure. Their three-dimensional aspect is explained in Sect. 4.4.

## 4. Three-dimensional configurations

The principal aim of the use of 3-D harmonics is the study of the magnetic configuration of the observed feet of prominences, that at periodic distance reach the photosphere. Démoulin et al. (1989) have attempted to understand prominence feet by using the 3-D harmonics of Eqs. (4–6): there the prominence was modelled by a massive current line and its vertical equilibrium in the linear force-free field was studied. In the present paper the approach is totally different: we look for magnetic configurations with dips (without extra addition of concentrated current).

### 4.1. The choice of the 3-D harmonics

For simplicity, we will only use some having  $n_y = 1$ , so that all of the periodic feet under the main body of the prominence

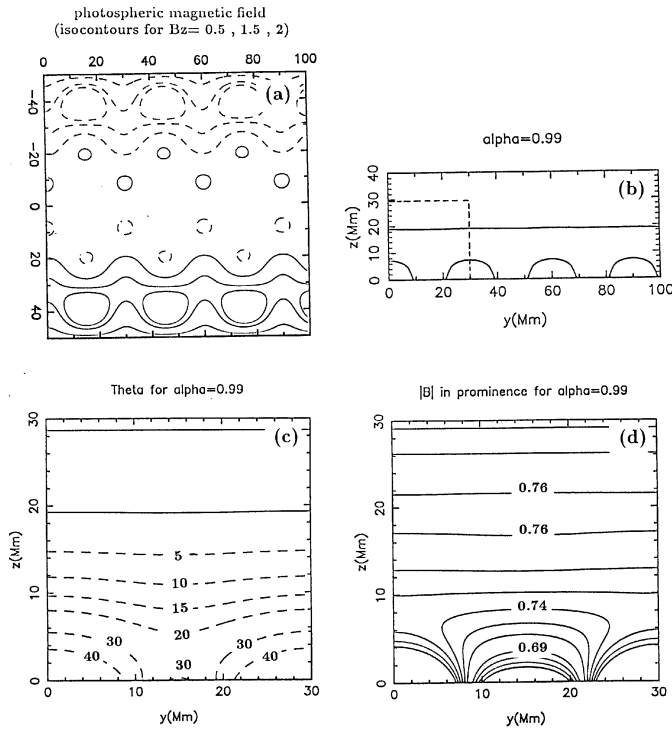


**Fig. 5a–d.** Different observable parameters for a typical OF configuration, with:  $\tilde{B}_{1,0} = 1$ ,  $\tilde{B}_{2,0} = -1.2$ ,  $\tilde{B}_{3,0} = 0.4$ ,  $\tilde{B}_{1,1} = 0$ ,  $\tilde{B}_{2,1} = 0.3$ ,  $\tilde{B}_{3,1} = -0.7$ ,  $\alpha = 0.99$ ,  $L_x = 100$  Mm,  $L_y = 30$  Mm. The vertical photospheric field is shown on **a**. Full lines are given for  $B_z > 0$  and dashed lines for  $B_z < 0$ . The field pattern is mainly bipolar, with a low field region containing some small parasitic polarities, between the two main polarities (presence of a corridor). **b** shows the prominence viewed from aside. The feet, that are due to the presence of bald patches, reach the photosphere with a periodicity of  $L_y = 30$  Mm, referring to the mean size of the supergranulation cells. **c** and **d** refer to the zoomed section of the prominence pointed out by dashed lines in **b**. The angle between the field and the prominence axis at  $x = 0$  is reported in **c**. It decreases with height, and becomes 0 at the top of the prominence (this is due to the twisted configuration), and it is maximum at low heights, in the feet.  $\theta$  changes its sign above the prominence, so the skew of the overlying arcades is opposite to the one in the prominence. The norm of the magnetic field is given in **d**. It increases with height inside the prominence, which is consistent with the presence of dips in the field lines.

will have the same height. Different values for  $n_y$  would mainly distinguish between suspended feet and feet that reach the photosphere. We use a set of six harmonics:

$$B_{x,y,z} = \sum_{n_x=1}^3 \sum_{n_y=0}^1 B_{x,y,z}(n_x, n_y). \quad (25)$$

We assume that the periodicity in the  $y$  direction is  $L_y = 30$  Mm, which is a suitable value for the size of the supergranulation cells. As in Sect. 3, we use  $L_x = 100$  Mm. This gives us a ratio of  $k_x/k_y = 0.3$ . For this value, the 2.5-D configuration is only an approximate guide of what is happening in 3-D.

In order to have prominence feet, we choose the amplitude of harmonics to have bald patches, appearing periodically in the

$y$  direction. It is clearly seen in Fig. 2 that the BP region stands around the line given by Eq. (21). So we will have to choose  $\tilde{B}_2$  and  $\tilde{B}_3$  according more or less to this equation. The choice for the amplitude of the harmonics is also restricted by the polarity of the photospheric field we want to deal with, especially a globally bipolar region is present in many observations. Then, we choose  $\tilde{B}_2$  and  $\tilde{B}_3$  so that we stay around the bipolar region (see Fig. 1a and b). As expected from the 2.5-D approach, the underlying feet, as the lateral ones, are due to the presence of small parasitic polarities in this low field corridor. The amplitude of the 3D harmonics are limited to keep the flux of these polarities inferior to those of the principal bipolar component.

The last constraint, but not the least, is brought by measurements of the angle made by the magnetic field and the prominence axis, observed by Hanle effect (in this paper we name this angle  $\theta$ ). Recent observational results show that for most prominences,  $\theta$  is in the order of  $10^\circ - 40^\circ$  (Bommier & Leroy 1997). In Fig. 4 is shown the maximum value of this angle inside a fully 3-D prominence for fixed values of  $\tilde{B}_{1,1}$  and  $\tilde{B}_{2,1}$  and  $\tilde{B}_{3,1}$ . One can see that this maximum value stands in the region of bald patches, where we expect the feet to be present. For low  $|\alpha|$ , we can get a quite large value of  $\theta$ , whatever is the choice for  $\tilde{B}_2$  and  $\tilde{B}_3$ . For larger  $|\alpha|$ , the reverse line, that marks the transition from FX to OF, appears (see Fig. 2). At this place,  $\theta(\text{reverse line}) = 0$ . This means that there the field is completely aligned with the photospheric inversion line. On both sides of the reverse line,  $|\theta|$  increases, in a normal (FX) or in an inverse (OF) polarity configuration. For higher values of  $|\alpha|$ , the highest values of  $|\theta|$  can be found in the OBP region. This is an interesting result, as it shows than even with a high  $|\alpha|$ , the angle made by the magnetic field and the prominence axis can be still significant, especially when the twisted configuration reaches the photosphere. This effect is due to the fact that the larger is  $n_x$ , the lower  $\alpha$  rotates the field in the  $y$ -direction and that at low height, for a large  $|\alpha|$ , the  $B_x$  component of the second and third harmonics dominate the first one.

#### 4.2. The commonly used OX configuration

It has been shown in previous sections that, with our assumptions, the FX configuration does not provide suitable characteristics for a prominence. So the magnetic configuration of prominences has to be modelled with a twisted flux tube. We first investigate the OX (see Fig. 3), by extending it to 3-D. This configuration has been introduced by Kuperus & Raadu (1974) as a suitable inverse polarity configuration for prominences. Then many studies have been built upon it in the field of prominences (see the review of Priest 1990) and coronal mass ejections (see Low 1996 and references therein), so that it has been commonly used as a 2.5-D configuration to describe a filament supported by a twisted flux tube. One has to note that the OX region in the  $(\tilde{B}_2, \tilde{B}_3)$  diagram in Fig. 2 is very small, even for very high values of  $\alpha$ . Hence it is not easy to get this configuration. Nevertheless we describe one configuration with the following parameters:

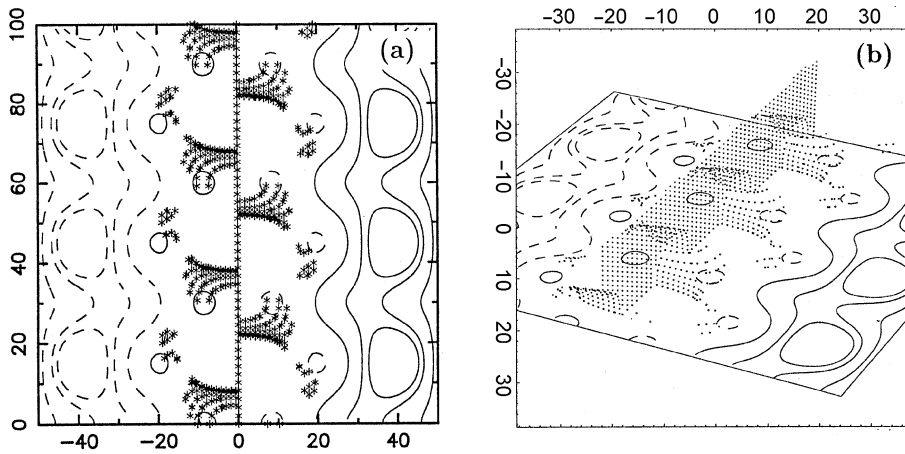


**Fig. 6a and b.** Location of dips in the field lines in three dimensions, above the computed magnetogram (full lines are given for  $B_z > 0$  and dashed lines for  $B_z < 0$ ) for the same parameters given for Fig. 5. **a** is the view from the top of the filament, and the dips are marked by stars. **b** is a perspective view, with the dips marked by small points. Note the lateral feet structures. They are located aside from the classical underlying feet of the prominence.

$$\begin{aligned} \tilde{B}_{1,0} &= 1 & \tilde{B}_{2,0} &= -1.2 & \tilde{B}_{3,0} &= 1.2 \\ \tilde{B}_{1,1} &= 0 & \tilde{B}_{2,1} &= 0.3 & \tilde{B}_{3,1} &= -0.7 \\ \alpha(\text{normalized}) &= 0.99 & L_x &= 100 \text{ Mm} & L_y &= 30 \text{ Mm}. \end{aligned}$$

Looking at the  $\theta$  isocontours from Fig. 4, it is clear that there will be a strong gradient of the angle between the prominence and the magnetic field inside it, as the amplitudes  $\tilde{B}_2$  and  $\tilde{B}_3$  vary due to the 3-D effects. In the lower part of the feet of the 3-D configuration, we can show that, with a great care in the choice of the harmonics, we can get a quite suitable value of  $\theta$ , around  $10^\circ$ . If we want to have a greater value, the amplitude of the harmonics in  $n_y$  should be much larger. But then the photospheric magnetic field would be inconsistent with observations. Furthermore, whatever it is at low heights,  $\theta$  falls rapidly to very small values in the main prominence body. There, its value is in the order of  $1^\circ$  or less, which is totally inconsistent with observations made by Hanle effect (e.g. Bommier et al. 1994). This problem would not appear if the constraint due to the presence of periodic feet that reach the photosphere would not exist. The only way to get good values for  $\theta$  for the OX configuration is to have a very low maximum height for the bottom of the prominence, so that it would be close to the bald patches regions almost everywhere. As this is not observed, the  $\theta$  constraint is a very strong argument against these configurations in 3-D.

Another problem with this configuration is that the lateral dips that are present for the FF and the OF configuration (see Sect. 3.5) do not appear for the OX topology. This is due to the morphology of the parasitic polarities in the low field region. Hence, a prominence supported by an OX topology is very thin, and does not have lateral feet structures. Some small filaments in active regions are observed to be very thin with surrounding fibrils oriented parallel to the inversion line (e.g. Martin 1990). Though, this is probably due to the small thickness of the low field region. High resolution observations still show lateral feet structures very close to the filament, which is consistent with a thin low field corridor.

In the present model, the OX topology does not fit for suitable observable parameters in a prominence. The presence of parasitic polarities in the region close to the inversion line natu-

rally leads to the OF configuration, which is after all the biggest region in the parameters space for high  $|\alpha|$  (see Fig. 2). On the other hand, one has to remember that if a OF twisted flux tube erupts, the effect of the parasitic polarities will decrease as the configuration rises and expands in the corona. So the topology could evolve to OX. The lateral feet will then shrink (as observed by Martin, private communication). Finally, if the so commonly used OX configuration does not stand for a stable prominence, it is still the best one that can be used for the description of eruptive prominences and coronal mass ejections. It can be formed by the eruption of a non-symmetrical OF configuration in which one lateral X point rises more rapidly than the other.

#### 4.3. Filaments in OF twisted flux tubes

Using the limitations given in Sect. 4.1, one can easily find many combinations of parameters that match the observed parameters for a suitable prominence. Here we only give one. We take a set of parameters that gives us a 2.5-D OF topology, close to the bald patches (for the presence of feet and large value of  $\theta$ ) and close to the bipolar region. We restrict the amplitude of 3-D harmonics (to get small parasitic polarities). The results with the parameters as above for the OX configuration, except that  $\tilde{B}_{3,0} = 0.4$ , are shown in Fig. 5a–d.

The computed magnetogram shown in Fig. 5a gives the value of  $B_z(z=0)$ , as it would be observed by a magnetograph that measures the normal component of the magnetic field. One can see a main bipolar region, with a low field corridor extending 20 Mm away on each sides of the inversion line, at  $x=0$ . The parasitic polarities inside this corridor naturally appear in an hexagonal pattern, which matches well with observed concentrated fields located at the edges of supergranules.

The location of the dips in the y-z plane is shown in Fig. 5b. It represents a low height prominence (around 20 Mm), with underlying feet that reach the photosphere every 30 Mm. A higher prominence can be achieved, either by increasing  $L_x$  or  $|\alpha|$ . This would respectively lead to quiescent prominence, or highly sheared active region prominence.

As measurements of the magnetic field inside the prominence give a strong constraint on the model, the norm of  $\mathbf{B}$

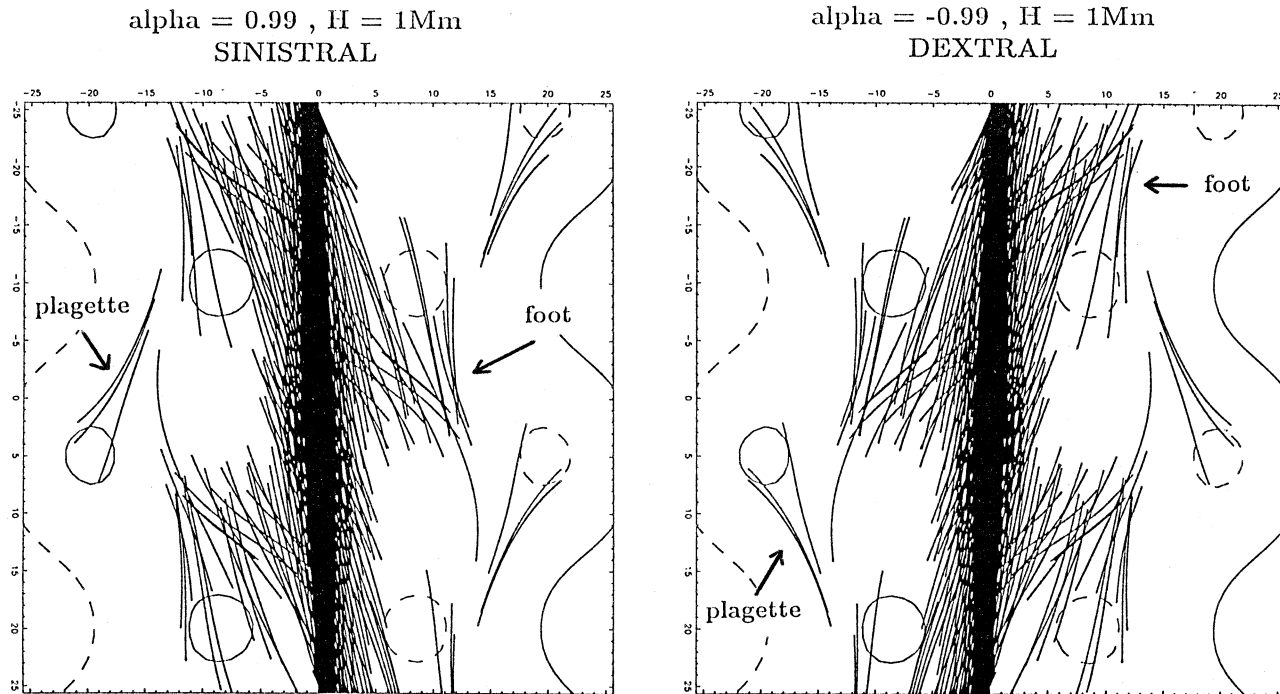


**Fig. 7.** Field lines computed for the same parameters than Fig. 5; they are drawn only at the dip locations shown in Fig. 6. Only the part of their dip which is supposed to be filled on a given height  $H = 1$  Mm is represented in order to simulate the appearance of cold material supported in the field. Note that the dextral and sinistral, as right and left bearing, configuration only depends on the sign of  $\alpha$ .

and the angle  $\theta$  inside the prominence are represented in Fig. 5d and c. The magnetic field slightly increases with height in the prominence, which is coherent with the presence of dips in the field lines. The value of the angle  $|\theta|$  decreases with height for this kind of twisted topology.

Up to now, we have only considered the presence of dips above the inversion line, in particular the underlying feet, despite of the presence of lateral dips in 2.5-D for the OF and OBP configurations (see Sect. 3.5). We compute the magnetic field in a cube of  $L_x^3$ , and we look for the dips everywhere in this region, using Eq. (16) (see Fig. 6a and b). Viewed from the top, these secondary dips are more or less located above the secondary inversion lines, that stand around the nearest parasitic polarities of the low photospheric field region. These lateral dips are located in between the prominence underlying feet and the parasitic polarities. They are not suspended features in the corona but reach the photosphere, forming bald patches. Another interesting feature that did not appear at all in 2.5-D is the presence of other smaller dip structures, further away from the prominence. They are also related to other small magnetic polarities, but they do not join the prominence.

#### 4.4. Fine structures in OF prominences

Assuming that the shape of the prominence is characterized by the presence of cold plasma contained in magnetic field-line dips, it is necessary to know which portion of these is likely to be filled with matter. A good approximation is to suppose that

the cold plasma fills a dip up to certain height which corresponds to the pressure height scale, given by:

$$H \simeq \frac{(1 + \xi)k_B T}{m_p g_\odot}, \quad (26)$$

where  $\xi = n_e/(n_p + n_n)$  the ionisation degree,  $k_B$  the Boltzmann constant,  $n_p$ ,  $n_n$  and  $n_e$  the proton, neutral hydrogen and the electron density,  $g_\odot$  the solar surface gravity, and  $T$  the temperature. For typical values for  $(\xi, T)$  in a prominence,  $H$  varies between 0.2 and 0.5 Mm. But, with macroscopic kinetic energy,  $H$  is likely to be higher. Taking this fact into account, we represent the portion of the field lines which can support plasma up to a height of  $H = 1$  Mm, at regular space locations where a dip is present in the magnetic configuration.

It is striking to see in Fig. 7 that some field lines not only appear inside the prominence body, but also aside from the prominence. Viewed from above, the lateral dip structures are composed of some portions of field lines, that look like what has been introduced as barbs by Martin et al. (1994). These structures match quite well those of observed regular filaments (see Fig. 8). They naturally appear periodically, in pairs, at every 30 Mm. Each pair corresponds to the presence of small parasitic polarities close to the prominence, and hence, to the void between two underlying feet (see Fig. 6b). Now let's focus on the shape of one pair of feet. The orientation, the shape and the proximity of the represented field lines give the first impression that some field lines can cross the prominence. This is not so. One can see in Fig. 9a and b that these two lateral features are

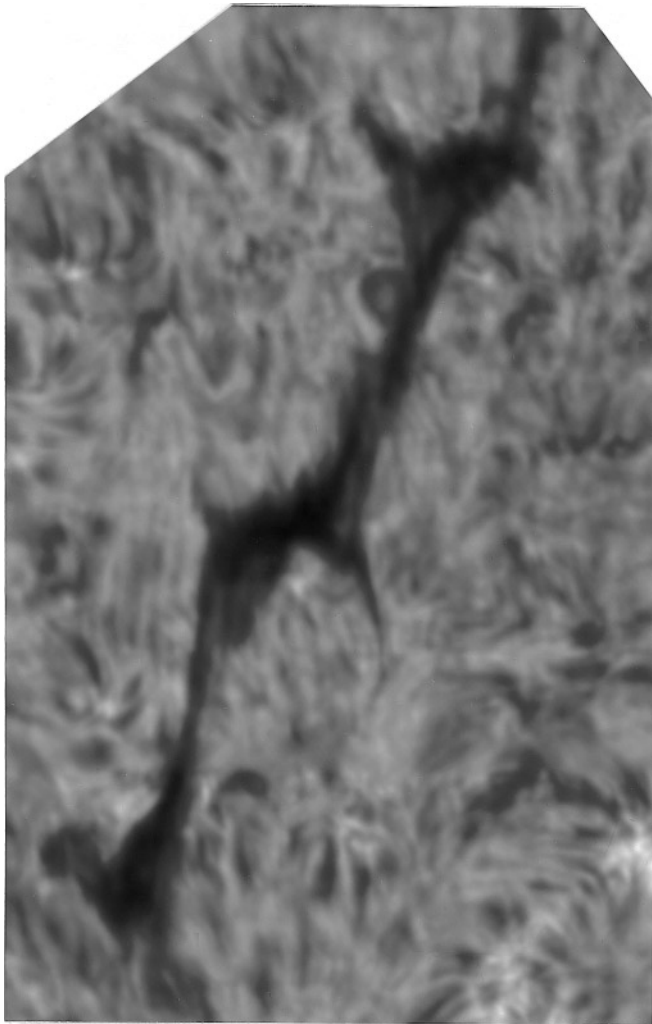


**Fig. 8.** Filament observed in  $H\alpha$  with the MSDP on the German VTT (Tenerife), on the 25 September 1996 (see courtesy Mein et al. 1997).

in fact composed of different field lines, each having a dip that can contain plasma.

There are also other dipoles at the edge of the photospheric low field region (in the filament channel). They are located at low height (Fig. 6a and b) and the associated fibrils seem to converge in the direction of the filament. This is due to an inversion of the  $B_x$  component. We got the fishbone structure present at the border of a flux tube embedded in an arcade as observed by Filippov (1994). We propose these structures as a possible explanation for plagues or dark fibrils around prominences (see Martin et al. 1994).

It is noteworthy that we focus here only on the dipoles, but at the chromospheric level dense material can be injected along field lines without dipoles. Then a representation like Fig. 7 may be completed by fibril-like objects which visualize the lower part of field lines filled dynamically with cold plasma. This has been realized by Low & Hundhausen (1995) in their Fig. 7. A similar pattern is present in our model, but with a modulation

in the  $y$  direction; we however choose to focus here only on the new aspect: the lateral dipoles.

It is obvious in Fig. 7 that a simple reversal of the sign of  $\alpha$  changes the orientation of the lateral feet: A positive value of  $\alpha$  gives a sinistral and left-bearing prominence, with overlying arcades having a right skew, and a right-handed helical field for the flux tube that supports the prominence. A negative  $\alpha$  gives a dextral and right-bearing prominence, with overlying arcades having a left skew, and a left-handed helical twist for the flux tube. This naturally links together the observed different patterns of chirality, in relation with the hemispheric helicity segregation (Martin et al. 1994; Rust & Kumar 1994; Pevtsov et al. 1995).

#### 4.5. Evolution with the shear

Let suppose that the magnetic helicity slowly accumulates in the magnetic configuration (see e.g. Rust & Kumar 1994). We now investigate the quasi-stationary evolution of a given structure defined as in Sect. 4.3, as we vary  $\alpha$  from 0 (potential case) to 1 ( $\alpha_{max}$ ). It can be clearly seen in Fig. 10 that for low  $|\alpha|$ , the configuration is FX, normal polarity, and that the prominence is very thin in height (a few Mm). The orientation of dark fibrils in the feet has not the observed direction (they are nearly orthogonal to the foot rather than along it). Furthermore, the prominence is interrupted along its axis. It is formed by a succession of feet without prominence “body”. Here we see that it is not easy to build a suitable FX configuration for a well developed prominence.

The interesting part of this evolution is when  $\alpha$  gets its critical value  $\alpha_{crit}$ , in other words when the reverse line crosses the point defined by  $(\vec{B}_2, \vec{B}_3)$ . We already know the properties of such an event for the 2.5-D case (see Sect. 3.3). Fig. 10 confirms that the magnetic field in the prominence aligns itself with the inversion line, as the prominence vertical extent decreases to zero. But what is new here is that this is also true in the full prominence corridor. From an observational point of view, this configuration will be composed of elongated fibrils, parallel to the inversion line, with no observable prominence, in a low field corridor around two major magnetic polarities. This is the signature of filament channels (e.g. Gaizauskas et al. 1997).

For higher values than  $\alpha_{crit}$ , the prominence becomes OF. It has the right observed chirality characteristics and the individual fibrils in the feet are approximately along their axis, as observed. As  $|\alpha|$  keeps increasing, we get a prominence whose top rises (see Démoulin & Priest 1989). With a value of  $\alpha$  close enough to  $\alpha_{max}$ , one can get dipoles up to heights as large as 50 Mm. The effect of  $\alpha$  is smaller at low height, where the first harmonic has a negligible contribution in  $B_x$ . Hence the feet are almost unaffected by  $\alpha$  in OF configurations (the properties of feet are mainly determined by the local parasitic polarities).

To conclude with this evolution, one has to stay aware that what we have shown here does not come from a full MHD treatment, which is far beyond the scope of this paper. The step from FX to OF is assumed to be due to reconnection processes. Does this evolution really take place on the sun or does the config-

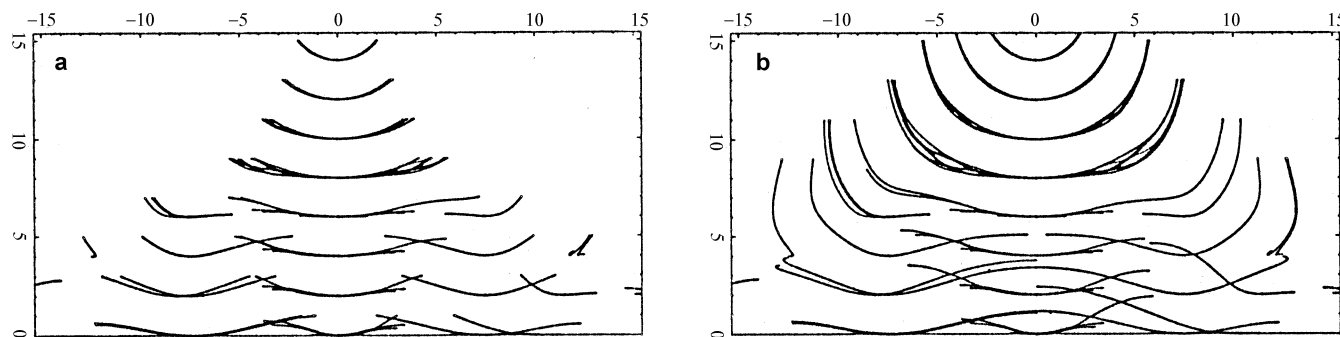


**Fig. 9a and b.** Prominence viewed in its axis direction (in the  $y$  direction), for different filling heights of the field lines.  $H = 1$  Mm for **a** and  $H = 5$  Mm for **b**. The field lines are only represented on the given height, around the bottom of their dip. Some of the lateral ones are very flat and asymmetric. Note that the dips that support the lateral feet do not cross the prominence axis. They are in fact composed of different field lines.

uration emerged twisted (so mainly in the OF configuration)? The first scenario can be validated only if one can observe the rotation of the fibrils in the feet as the prominence is forming or if one can justify the absence of significant dense material in the FX case so that this kind of prominence would be only weakly visible in projection on the solar disk. The small extension in height contributes to this, but is it sufficient?

## 5. Conclusions

The magnetic configurations suited for prominence support we derived in the present Paper are based on few hypotheses only; we supposed that:

- the coronal and prominence plasmas have a low plasma  $\beta$ , so we can neglect effects of plasma (dynamics, pressure and gravity) at first order, and consider force-free field configurations;
- the cold prominence material is supported in magnetic dips;
- the helicity is negative (resp. positive) in the northern (resp. southern) hemisphere (as observed, e.g. Seehafer 1990; Pevtsov et al. 1995);

- there is a quasi-periodic variation of the photospheric field along the prominence axis (due to supergranulation cells).

All these hypotheses, except the presence of magnetic dips, are well supported by observations. The dip hypothesis, the main one in our model, has mainly theoretical grounds (the free-fall time of dense plasma being much too short, and a clear velocity signature of free fall being absent in observations). Observational evidence for dips is present during eruptions only (e.g. Rompolt 1990), or in magnetic field measurements via the Hanle effect (e.g. Bommier et al. 1994). This hypothesis is justified a posteriori in the model for the quiescent phase of prominences by the natural presence of lateral feet exhibiting certain observed morphological characteristics. Of less importance is the hypothesis of force-free fields. Because of the prominence and coronal conditions, this gives a first order approximation which can be only slightly modified by introduction of plasma of the observed density. We further restrict our analysis to linear force-free fields in order to investigate a large class of solutions (in particular with those of various photospheric vertical field distributions).

Using this first order approach, which reproduces the main features of a 3-D twisted configuration, and the four above mentioned hypotheses, we can reproduce the following disjointed observations:

*At photospheric and chromospheric levels, there exist:*

- A low field gradient in the corridor (e.g. Maksimov & Prokopiev 1995, and references there in);
- A large photospheric and chromospheric magnetic shear (e.g. Martin 1986; Rompolt 1990);
- Chromospheric fibrils which are not crossing the photospheric inversion line (Martin 1990);
- A fishbone structure of  $H\alpha$  fibrils on both side of the inversion line as observed by Filippov (1994).

*The Magnetic field measurements imply that:*

- The field is nearly horizontal (e.g. Athay et al. 1983);
- The component of the field along the prominence axis is dominant (e.g. Bommier et al. 1986);
- Both horizontal magnetic components are directed in a way opposite to that of an arcade which would have been sheared by differential rotation (e.g. Bommier et al. 1994);
- The field strength increases with height (e.g. Leroy et al. 1983).

*The Chirality patterns and feet organization are:*

- The magnetic configuration is dextral with  $\alpha < 0$  (as observed in the northern hemisphere);
- Dextral (resp. sinistral) chirality is always associated to right (resp. left) bearing prominences (Martin et al. 1994);
- The overlying coronal arcade is left-bearing for a dextral filament (Martin & Mc Allister 1995)
- Feet alternate between both side of the prominence;
- Feet end at the close vicinity of the parasitic polarities which are present in the corridor (Martin et al. 1994);
- Feet are formed by dense material supported in shallow magnetic dips distinct from the ones forming the main prominence body (Forbes, private communication).

While the present model is based on linear force-free fields, one can still outline the basic observational consequences of a quasi-stationary evolution in an emergence/relaxation context:

- Converging and canceling magnetic features around the inversion photospheric line (Martin 1986; Low & Hundhausen

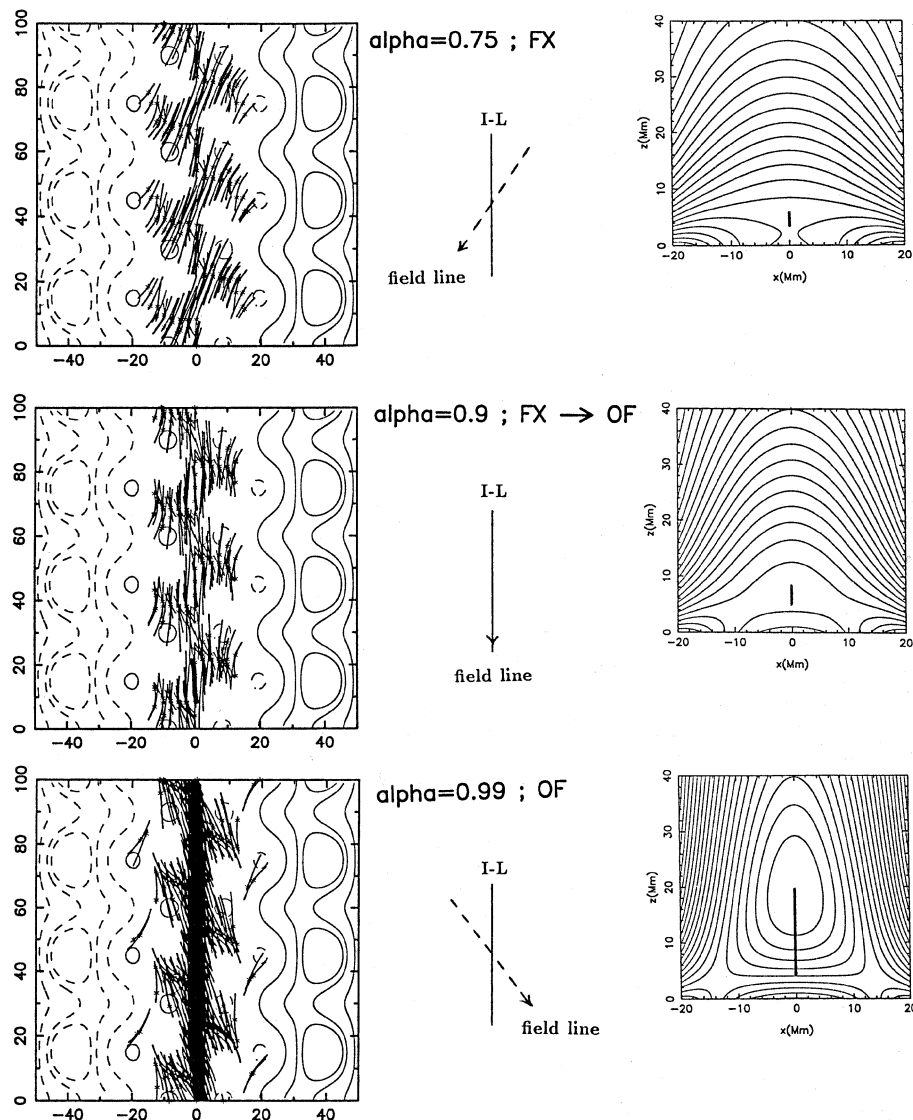


**Fig. 10.** Evolution of the topology with  $\alpha$  for the set of parameters given in Fig. 5. For lower values of  $\alpha$ , the topology is FX and the magnetic configuration is normal. For higher values of  $\alpha$  the topology is OF and the magnetic configuration is inverse. For a critical value  $\alpha_{crit}$ , the topology passes from FX to OF. There, the field is parallel to the inversion line, almost everywhere in the low field region, and the prominence vertical thickness is null. This could be observed as an empty filament channel.

1995);

- Continuous lift up of chromospheric material in the feet (above bald patches, see Titov et al. 1993). The total prominence mass can be much greater than the deficit of mass in the prominence cavity;

- The prominence feet form first in the model with an increasing helicity (as observed by Martres et al. 1966);

- The magnetic field field lines are flat and nearly aligned with the prominence axis, in particular at the top of the prominence (O point in a perpendicular cut). So, there, any plasma pressure difference will drive expected plasma motions along the prominence axis (e.g. Athay 1990);

- Because of the shallow dips in feet, a slight evolution of the configuration can produce a downward drainage of part of the cold material (as seen in  $H\alpha$  prominence movies; see also Schmieder 1989)

- Because of their intrinsic link to parasitic polarities, feet are expected to evolve with a typical supergranule lifetime (around one day, Martin 1997);

- This contrast with the slow evolution expected for the main prominence body: this evolution is linked to the average magnetic flux in the main photospheric polarities (in accordance with Hanle measurement: Leroy 1989).

Finally we note how fundamental the three-dimensional nature of the model was for the present study. It is obviously important for comparison with observations, but moreover it shows us the importance of the OF configurations (which in 2.5-D models appear only more complicated than OX configurations). We have also shown the importance of feet (a well-known aspect to observers!): they appear to be the main location for prominence material supply in the context of an emerging flux tube. The topology of the magnetic configuration is interesting by itself, since both separatrices associated to the bald patches as well as quasi separatrix layers are present. Hence, driven reconnection is thought to be present below the feet (lift-up of material) and in between the feet at the prominence bottom (it can explain the sharp bottom edge of the prominence and the bright rim ob-

served below). This will be the object of the next paper with an emphasis on the feet evolution.

*Acknowledgements.* The authors thank Wim van Driel and Lidia van Driel-Gesztelyi for their help in the improvement of the manuscript.

## References

- Amari T., Aly J.J. 1992, *A&A* 265, 791  
 Amari T., Démoulin P., Browning P., Hood A.W., Priest E.R. 1991, *A&A* 241, 604  
 Antiochos S.K., Dahlburg R.B., Klimchuck J.A. 1994, *ApJ* 420, L41  
 Athay R.G. 1990, *Solar Phys.* 126, 135  
 Athay R.G., Querfeld C.W., Smartt R.N., Landi Degl'Innocenti E., Bommier V. 1983, *Solar Phys.* 89, 3  
 Bommier V., Leroy J.L. 1997, in D. Webb, B. Schmieder and D. Rust (eds.), *IAU Colloq.* 167, *PASP*, in press  
 Bommier V., Leroy J.L., Sahal-Bréchet S. 1986, *A&A* 156, 79  
 Bommier V., Landi Degl'Innocenti E., Leroy J.L., Sahal-Bréchet S. 1994, *Solar Phys.* 154, 231  
 Choe G.S., Lee L.C. 1992, *Solar Phys.* 138, 291  
 d'Azambuja L., d'Azambuja M. 1948, *Annales de l'Observatoire de Paris*, 6, 7  
 Démoulin P., Priest E.R. 1989, *A&A* 214, 360  
 Démoulin P., Priest E.R., Anzer U. 1989, *A&A* 221, 326  
 Fiedler R.A.S., Hood A.W. 1993, *Solar Phys.* 146, 297  
 Filippov B.P. 1994, *Astron. Letters* 20, 665  
 Foukal P. 1971, *Solar Phys.* 19, 59  
 Gaizauskas V., Zirker J.B., Sweetland C., Kovacs A. 1997, *ApJ* 479, 448  
 Inhester B., Birn J., Hesse M. 1992, *Solar Phys.* 138, 257  
 Kim I.S. 1990, in V. Ruždjak, E. Tandberg-Hanssen (eds.), *IAU Colloq.* 117, Springer-Verlag, 49  
 Kippenhahn R., Schlüter A. 1957, *Zs. Ap.* 43, 36  
 Kuperus M., Raadu M.A. 1974, *A&A* 31, 189  
 Leroy J.L. 1988, in R.C. Altrock (ed.), *Solar and Stellar coronal structures and dynamics*, National Solar Observatory, 422  
 Leroy J.L. 1989, in E.R. Priest (ed.), *Dynamics and Structure of Quiescent Solar Prominences*, Kluwer Academic Publishers, Dordrecht, Holland, 77  
 Leroy J.L., Bommier V., Sahal-Bréchet S. 1983, *Solar Phys.* 83, 135  
 Leroy J.L., Bommier V., Sahal-Bréchet S. 1984, *A&A* 131, 33  
 Low B.C. 1994, *Plasma Phys.*, 1, 1684  
 Low B.C., Hundhausen J.R. 1995, *ApJ* 443, 818  
 Low B.C. 1996, *Solar Phys.* 167, 217  
 Maksimov V.P., Ermakova L.V. 1985, *SvA* 29(3), 323  
 Maksimov V.P., Prokopiev A.A. 1995, *Astron. Nachr.*, 4, 249  
 Malherbe J.M. 1989, in E.R. Priest (ed.), *Dynamics and Structure of Quiescent Solar Prominences*, Kluwer Academic Publishers, Dordrecht, Holland, 115  
 Martin S.F. 1986, in A. Poland (ed.), *CPP NASA Conference*, C.P. 2442, 73  
 Martin S.F. 1990, in V. Ruždjak, E. Tandberg-Hanssen (eds.), 1990, *IAU Colloq.* 117, Springer-Verlag, 1  
 Martin S.F. 1997, in D. Webb, B. Schmieder and D. Rust (eds.), *IAU Colloq.* 167, *PASP*, in press  
 Martin S.F., Bilimoria R., Tracadas P.W. 1994, in R. Rutten and C. Schrijvers (eds.), *Solar Surface Magnetism*, Kluwer Ac. Pub., 303  
 Martin S.F., Mc Allister A.H. 1995, in *Proc. Colloq. IAU 153, Magnetodynamics Phenomena in the Solar Atmosphere*  
 Martres M.J., Michard, R., Soru-Escout, I., 1966, *Ann. Astrophys.* 29, 249  
 Mein P., Wiik J.E., Schmieder B., et al. 1997, in D. Webb, B. Schmieder and D. Rust (eds.), *IAU Colloq.* 167, *PASP*, in press  
 Nakagawa Y., Raadu M.A., 1972, *Solar Phys.* 25, 127  
 Pevtsov A.A., Canfield R.C., Metcalf T.R. 1995, *ApJ* 440, L109  
 Priest E.R. 1990, in V. Ruždjak, E. Tandberg-Hanssen (eds.), 1990, *IAU Colloq.* 117, Springer-Verlag, 150  
 Priest E.R., Hood A.W., Anzer U. 1989, *ApJ* 344, 1010  
 Raadu M.A., Schmieder B., Mein N., Gesztelyi L. 1988, *A&A* 197, 289  
 Rompolt B. 1990, *Hvar Obs. Bull.* Vol. 14, 1, 37  
 Rust D.M., Kumar A. 1994, *Solar Phys.* 155, 69  
 Schmieder B. 1989, in E.R. Priest (ed.), *Dynamics and Structure of Quiescent Solar Prominences*, Kluwer Academic Publishers, Dordrecht, Holland, 15  
 Schmieder B., Raadu M.A., Wiik J.E. 1991, *A&A* 252, 353  
 Seehafer N. 1990, *Solar Phys.* 125, 219  
 Shelke R.N., Pande M.C. 1983, *Bull. Astr. Soc. India*, 11, 327  
 Titov, S. Priest, E.R., Démoulin P. 1993, *A&A* 276, 564  
 Van Ballegoijen A.A., Martens P.C.H. 1989, *ApJ* 343, 971  
 Vršnak B., Ruždjak V., Rompolt B. 1991, *Solar Phys.* 136, 151

This article was processed by the author using Springer-Verlag L<sup>A</sup>T<sub>E</sub>X A&A style file L-AA version 3.